Oceanologia 64 (2022) 583—594

Available online at www.sciencedirect.com

ScienceDirect

journal homepage: www.journals.elsevier.com/oceanologia

ORIGINAL RESEARCH ARTICLE

# Dynamics of absorption properties of CDOM and its composition in Likas estuary, North Borneo, Malaysia

**Saiyidah Munirah Mohd-Shazali[a], Jafar-Sidik Madihah[a,*], Nurzaliah Ali[a], Chen Cheng-Ann[a], Robert J.W. Brewin[b], Md. Suffian Idris[c], P. Purba Noir[d]**

[a] *Borneo Marine Research Institute, University of Malaysia of Sabah, Sabah, Malaysia*
[b] *Centre for Geography and Environmental Science, College of Life and Environmental Sciences, University of Exeter, Penryn, Cornwall, United Kingdom*
[c] *Faculty of Science and Marine Environment, University of Malaysia Terengganu, Terengganu, Malaysia*
[d] *Marine Research Laboratory (MEAL), Faculty of Fishery and Marine Science, Padjadjaran University, Jatinangor, Indonesia*

Received 18 May 2021; accepted 15 April 2022
Available online 17 May 2022

**KEYWORDS**
Coloured dissolved organic matter (CDOM);
The absorption coefficient of CDOM (aCDOM);
Molecular weight and degradation of CDOM;
High molecular weight (HMW) CDOM;
Low molecular weight (LMW) CDOM

**Abstract** Chromophoric Dissolved Organic Matter (CDOM) is a vital water constituent in aquatic ecosystems that contributes to water colour, affects light penetration, and impacts primary production. This study aims to determine the spatial and monsoonal variability of CDOM absorption properties in the Likas estuary, characterise the source of CDOM, and investigate the correlations between CDOM absorption properties and salinity. Likas estuary is a small estuary located in Kota Kinabalu city on the west coast of Sabah, facing the South China Sea. A mangrove ecosystem surrounds it with manufactured structures such as residential areas and public facilities. Surface water samples were collected at 19 stations: upstream of rivers to the river mouth and coastal area during spring tides every month, from June 2018 to July 2019, for 14-months. The distribution of $a_{CDOM}(440)$ in the study area is predictable as a signature in a coastal area with a decreasing gradient from the upstream towards coastal water ($0.29 \pm 0.19$ $m^{-1}$ to $1.05 \pm 0.39$ $m^{-1}$). There are increasing spatial patterns of spectral slopes $S_{275\text{-}295}$ and $S_R$. However, $S_{350\text{-}400}$ and $S_{300\text{-}600}$ declined spatial gradients from the upstream to coastal water. Thus, $S_{300\text{-}600}$ indicates a linear relationship between $a_{CDOM}(440)$, which unconventional results

* Corresponding author at: Borneo Marine Research Institute, Universiti Malaysia Sabah, Jalan UMS 88400, Kota Kinabalu, Sabah, Malaysia.
*E-mail address:* madihah@ums.edu.my (J.-S. Madihah).
Peer review under the responsibility of the Institute of Oceanology of the Polish Academy of Sciences.

Production and hosting by Elsevier

https://doi.org/10.1016/j.oceano.2022.04.005
0078-3234/© 2022 Institute of Oceanology of the Polish Academy of Sciences. Production and hosting by Elsevier B.V. This is an open access article under the CC BY-NC-ND license (http://creativecommons.org/licenses/by-nc-nd/4.0/).

in coastal water. We suspect this is due to a small coverage of the study site with a distance of 0.5 m intervals of each station. This could be why the $S_{300-600}$ had constant values throughout the study area (with no statistical difference between stations). In addition, $S_{300-600}$ was merely varied in the stations located at the river mouth and coastal water. Based on the spectral slope ratio ($S_R$), most of the stations located in the Darau, Inanam, and Bangka-Bangka rivers had $S_R$ values less than 1. Hence, CDOM in these stations is a terrestrial-dominated source. Therefore, from our observations during the study period, monsoonal variation could alter the source of CDOM in the study area.
© 2022 Institute of Oceanology of the Polish Academy of Sciences. Production and hosting by Elsevier B.V. This is an open access article under the CC BY-NC-ND license (http://creativecommons.org/licenses/by-nc-nd/4.0/).

## 1. Introduction

Chromophoric Dissolved Organic Matter (CDOM) is a fragment of Dissolved Organic Matter (DOM) with chromophores molecules that absorb visible and ultra-violet (UV) light. CDOM contributes to the colour of natural water, with water with high CDOM concentration appearing brown as it absorbs UV preferentially, then blue and green regions of the light spectrum (Coble and Nelson, 2009; Kirk, 1994). The sources of CDOM vary from being allochthonous to autochthonous. The allochthonous sources are mainly from the decomposition of terrestrial vegetation and soil by rivers and wetlands that carry decomposed terrestrial plants, sewage, and sediments or known as a terrestrial-dominated source of CDOM. Whereas autochthonous results from in-situ biological activity such as the production of aquatic primary producers, namely phytoplankton and zooplankton (Bowen et al., 2017; Brandão et al., 2018; Minu et al., 2020), which is associated with a marine-dominated source of CDOM. CDOM has also been used as a natural tracer to study the dispersion, transport, and mixing of water masses (Nelson et al., 2007; Stedmon et al., 2010).

CDOM can act as a protective barrier in shielding biota and coral reefs from damaging UV radiation in shallow coastal areas due to its strong absorption of UV light. However, the increasing supply of CDOM concentration by rivers can affect underwater light availability, reducing the photic depth and causing light limitation for phytoplankton, impacting primary production and surface ocean heating by altering the energy and heat budget of coastal waters (Granskog et al., 2007; Guèguen et al., 2005; Nelson et al., 1998). The optical properties of CDOM that can provide information on DOM and DOC are useful for quantifying carbon transport and continuous monitoring of wastewater discharge (Ferrari, 2000; Shanmugam et al., 2016).

The spectral shape of CDOM can also be used to help separate the absorption of phytoplankton, detritus, and minerals and provide insights into CDOM composition (Grunert et al., 2018). CDOM plays an essential role in assessing water quality and biogeochemical cycling (Andrew et al., 2013; Hickman et al., 2010; Kim et al., 2016). The spectral characteristics of CDOM absorption provide valuable insights into the composition and origins of CDOM and allow retrievals of CDOM in coastal and estuarine waters from ocean colour remote sensing (Grunert et al., 2018; Menon et al., 2011). The spectral slope parameter (S) of CDOM describes the spectral dependence of the CDOM absorption coefficient with wavelength and can provide information on the source of CDOM and its susceptibility to biological and photochemical processes (Blough and Del Vecchio, 2002; Osburn and Stedmon, 2011; Stedmon and Markager, 2001). The S value has also been related to the molecular weight and aromaticity of DOM (Blough and Green, 1995; Helms et al., 2008). For instance, the spectral slope between 275—295 nm ($S_{S275-295}$) is a good indicator of the different CDOM pools, marine and terrestrial (Grunert et al., 2018; Helms et al.,2008; Nima et al., 2019; Stedmon and Markager, 2001). The slope ratio (SR) of $S_{275-295}$ and $S_{350-500}$ (subscript reflects the wavelength range in nm) have also been shown to be useful for characterising CDOM in natural waters, with lower relative values indicative of DOM of higher molecular weight, greater aromaticity and increasing vascular plant inputs (Helms et al., 2008; Osburn et al., 2012; Spencer et al., 2010a).

The Darau River is a part of the Likas estuary. It is bounded by a large stretch of mangrove forest distributed from upstream towards the river mouth, with a few residential areas. The coastal and river mouth receives terrestrial input from three rivers: the Darau River, Bangka-Bangka River, and Inanam River. In addition, there is a wide range in salinity in the study area, resulting from the mixing of inflowing coastal water with outflowing freshwater. Due to these particular conditions, it is hypothesised that the CDOM pool may have different origins and compositions in the study area. The aims of this study are to 1) determine, for the first time, the spatial variability of CDOM absorption and spectral composition to help characterise its source; and 2) investigate correlations between CDOM absorption properties, spectral slopes, and salinity in the study region. Results will provide better insights into the dynamics of CDOM in the region and for the future development of regional remote-sensing algorithms of water colour.

## 2. Methodology

### 2.1. Study area and plan of sampling

The study was conducted in the Likas estuary, Kota Kinabalu, which is located on the west coast of Sabah and faces the South China Sea. The Likas Estuary is a small estuary surrounded by urban development influenced by mixed-tidal action. It receives water input from several connected rivers, such as the Darau River, Inanam River, and Bangka-Bangka River. The study area stretched about 2 km to 5 km

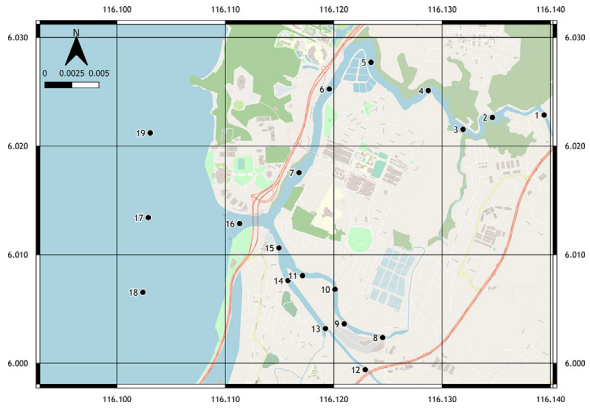


**Figure 1** The map of Darau river with 19 sampling points (black dots) that distributed from upstream of Darau river towards the coastal area of Likas estuary, Kota Kinabalu, Sabah.

in length, which measured from the river mouth towards the upstream Darau River, Bangka-Bangka River, and Inanam River. The study area is bounded by natural features such as a single large stretch of mangrove forest and manufactured structures, such as fisherman villages and developments. Another aspect is the variability in surface salinity exhibited in this region (from 0.13 ppt to 31.83 ppt) due to substantial freshwater input.

The climate in Kota Kinabalu is hot and humid, having an equatorial climate with consistent temperatures throughout the year, influenced by monsoon circulation. The Northeast monsoon (NEM) is driven by northeasterly winds and brings cool temperatures and less rainfall between November and March. The Southwest monsoon (SWM) is driven by southwesterly winds and brings warm temperatures but more rainfall between May and September. These two distinct monsoon seasons are separated by shorter two intermonsoon periods that take place from April to May (summer inter-monsoon) and from September to October (fall intermonsoon) (Teong et al., 2017). The tropical climate influences changes in the physicochemical conditions in tropical estuaries, such as rainfall, humidity, solar radiation, air temperature, and wind direction (Teong et al., 2017).

The sampling was carried out on a monthly basis starting from June 2018 until July 2019. There were 19 sampling points that were located from the upper stream of rivers towards the river mouth and coastal area of Likas estuary. The sampling was carried out in the daytime during spring tide. The surface water samples were collected for further laboratory analyses (Figure 1).

## 2.2. Determination of CDOM absorption coefficient and spectral slopes

For precautions, the collected surface water for CDOM analysis was stored in amber bottles and kept refrigerated before analysis in the laboratory. Before absorption analysis, water samples were filtered through a 0.2 μm cellulose nitrate membrane filter. Pure water was used as a blank to determine the CDOM absorbance of samples for wavelengths between 220 nm to 750 nm at 1 nm intervals using a UV-Vis DR 500 Hach spectrophotometer with a 10 cm quartz cuvette. CDOM absorbance was assumed to be zero for wavelengths above 700 nm. Therefore, the average CDOM absorbance for the interval between 700 nm to 750 nm was subtracted from the spectrum to correct for offsets due to instrument baseline drift, temperature and scattering effects (Green and Blough, 1994). The absorbance values were transformed into the absorption coefficient according to Helms et al. (2008), where the CDOM absorption coefficient, $a_{CDOM}(\lambda)$ in $m^{-1,}$ was calculated according to

$$a_{CDOM}(\lambda) = 2.303^{*}O_{CDOM}(\lambda)/\ l, \quad (1)$$

where l is the path length of the optical cell in meters, $a_{CDOM}(\lambda)$ is the absorption coefficient of CDOM at a given wavelength, and $O_{CDOM}(\lambda)$ is the absorbance at a given wavelength, from 300 nm to 600 nm. In this study, the CDOM absorption coefficient at a single wavelength of 440 nm ($a_{CDOM}(440)$) is used to describe the changes in CDOM quantity and to examine the spatial variability of CDOM within the studies area. The magnitudes of CDOM were measured by the absorption coefficient of CDOM, $a_{CDOM}(440)$. The absorption coefficient at 440 nm is chosen because it is the midpoint of the blue waveband peak that is related to the photosynthetic action spectrum of most classes of algae. It is also a wavelength measured by many ocean-colour satellites.

The CDOM spectral slope was determined by fitting the absorption coefficients to a single-exponential non-linear curve, to the wavelengths from 300 nm to 600 nm, using the equation of Bricaud et al. (1981), such that

$$a_{CDOM}(\lambda) = a_{CDOM}(\lambda r)\ \exp\ (-S_{CDOM}\ [\lambda - \lambda r]), \quad (2)$$

where $S_{CDOM}$ is the spectral slope of $a_{CDOM}$ and $\lambda_r$ is the reference wavelength at 440 nm. CDOM spectral characteristics and its spectral slope are typically indicative of the chemical composition of CDOM (Helms et al., 2008; Stedmon and Markager, 2001). The spectral slopes for intervals of 275—295 nm ($S_{275\text{-}295}$) and 350—500 nm ($S_{350\text{-}500}$) were calculated by fitting the log-transformed CDOM absorption coefficient to linear regression. Higher slopes indicate a more rapid decrease in CDOM absorption with increasing wavelength. The slope ratio ($S_R$) between $S_{275\text{-}295}$ and $S_{350\text{-}500}$ was also calculated. These wavelengths were chosen to help determine the composition and source of CDOM in the study area.

## 2.3. Statistical analysis

The statistical analysis was carried out using IBM SPSS Statistics 25 software. The normality of the dataset was checked by using the Shapiro-Wilk (SW) test to determine if the response variable of each group of data had a normal distribution. Based on the distribution pattern of each variable, one-way ANOVA (for a normal distribution) or the Kruskal-Wallis test (for non-normal distributions) were used to test for significant differences among study areas and between monsoons. The correlation coefficient (r) was determined from the regression analysis to study the relationship between CDOM, optical properties, and salinity.

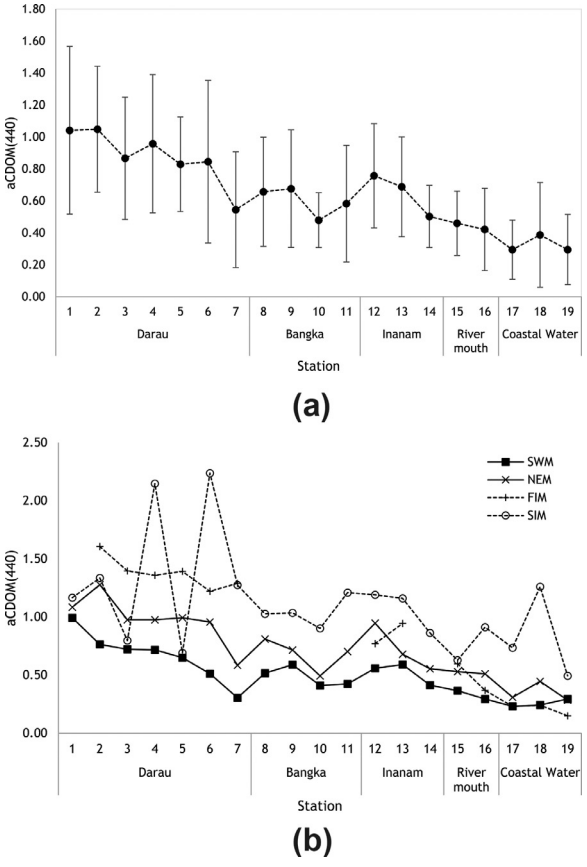


**Figure 2** The temporal and monsoonal mean of $a_{CDOM}(440)$ at each station during 14-month observation in the study area. Error bars in Figure 2a indicated standard deviation of the 14-month observation means.

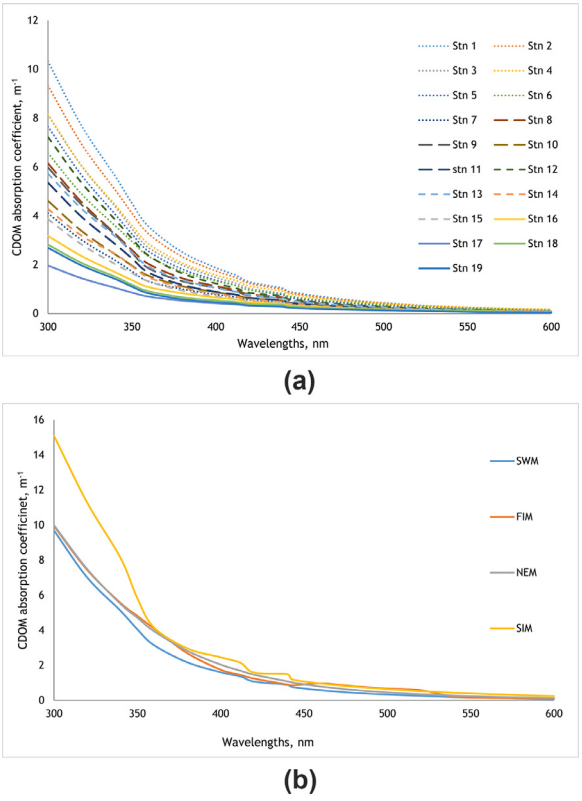


**Figure 3** Mean CDOM absorption spectra obtained by averaging over absorption coefficient from 300–600 nm and fitted to non-linear exponential decay function for a) Spatial distribution at 19 sampling stations and b) the monsoonal distribution during Southwest monsoon (SWM), FIM (Fall-Intermonsoon), Northeast Monsoon (NEM) and Summer Intermonsoon (SIM) during the study period.

## 3. Results

### 3.1. Spatio-temporal variations of $a_{CDOM}(440)$

The temporal mean $a_{CDOM}(440)$ varied between 0.29±0.19 $m^{-1}$ (station 17) at coastal water and 1.05 ± 0.39 $m^{-1}$ (Station 2) upstream of Darau, as plotted in Figure 2a. There was an apparent spatial gradient of $a_{CDOM}(440)$ in the study area that was relatively higher upstream (Station 1, 2, 8, and 12) compared to the station in the coastal area (Station 17, 18, and 19). The spatial distribution of $a_{CDOM}(440)$ showed statistically significant differences between sampling points ($p < 0.05$), where the $a_{CDOM}(440)$ decreased from the river to the coastal area ($p < 0.05$).

The monsoonal mean of $a_{CDOM}(440)$ was relatively low and had a decreasing pattern from the upstream to the coastal water during SWM with the range of 0.23 $m^{-1}$ (Station 17) and 0.99 $m^{-1}$ (Station 1) (Figure 2b). SIM, on the other hand, had a greater $a_{CDOM}(440)$, which fluctuated between 0.49 $m^{-1}$ (Station 19 — coastal area) and 2.24 $m^{-1}$ (Station 6 — Darau), with the value of $a_{CDOM}(440)$ nearly twice in SWM (Figure 2b). The monsoonal distribution of $a_{CDOM}(440)$ showed statistically significant differences between monsoons ($p < 0.05$).

### 3.2. CDOM absorption spectra

The CDOM absorption coefficient showed a decreasing trend in response to spatial and monsoonal variations (Figure 3). Figure 3 illustrates the mean absorption spectra of CDOM at all stations (Figure 3a) and the slope of monsoonal variations in the study area (Figure 3b). The spatial-spectral slope was higher at Station 1, located upstream of the Darau River ($S = 0.015$ $nm^{-1}$), whereas the lowest spectral slope was found at station 17 in the coastal water ($S = 0.011$ $nm^{-1}$), as plotted in Figure 3a.

For monsoonal trend, SIM monsoon attributed lower spectral slope with 14 $\mu m^{-1}$, primarily bigger CDOM absorption coefficient at 300 to 350 nm than other observed monsoons (Figure 3b). In contrast, an identical slope with small difference was observed during SWM ($S = 0.016$ $nm^{-1}$), FIM ($S = 0.015$ $nm^{-1}$) and NEM ($S = 0.015$ $nm^{-1}$) monsoons (Figure 3b).

### 3.3. Spectral slope $S_{275\text{-}295}$, $S_{350\text{-}500}$, and $S_R$ of absorption properties

The spatial means of CDOM spectral slope from 275 to 295 nm ($S_{275\text{-}295}$) had smaller differences between stations, ranging from 0.015 ± 0.002 $nm^{-1}$ (Station 1, upstream Darau

River) to 0.019 ± 0.010 $nm^{-1}$ (Station 17, coastal water), as illustrated in Figure 4a. However, when compared to other stations, Station 7 (Darau) and Station 13 (Inanam) showed a substantial standard deviation of 0.019 ± 0.010 $nm^{-1}$ and 0.017 ± 0.005 $nm^{-1}$ (Figure 4a) compared to other stations. Nevertheless, the spatial distribution of $S_{275\text{-}295}$ showed significant differences where $S_{275\text{-}295}$ increased from the river to the coastal area ($p<0.05$). The monsoonal means of $S_{275\text{-}295}$ peaked at Station 7 (Darau) during SWM (0.023 $nm^{-1}$) and Station 11 (Bangka) during SIM (0.024 $nm^{-1}$), as shown in Figure 4b. The monsoonal range of $S_{275\text{-}295}$ indicated relatively higher were coastal area with the ranges of 0.014 $nm^{-1}$ to 0.023 $nm^{-1}$ (SWM), 0.015 $nm^{-1}$ to 0.018 $nm^{-1}$ (NEM), 0.015 $nm^{-1}$ to 0.020 $nm^{-1}$ (FIM) and 0.015 $nm^{-1}$ to 0.024 $nm^{-1}$ (SIM) (Figure 4b). No significant differences were observed in the distribution of $S_{275\text{-}295}$ between monsoons ($p > 0.05$).

As shown in Figure 4c, the spectral slope from 350 to 400 nm ($S_{350\text{-}400}$) displayed a fluctuating pattern with a range of 0.015 ± 0.003 $nm^{-1}$ (coastal water station) to 0.019 ± 0.002 $nm^{-1}$ (upstream) as shown in Figure 4c. $S_{350\text{-}400}$ of Darau, and Inanam rivers showed a declining pattern, ranging from 0.017 ± 0.002 $nm^{-1}$ to 0.016 ± 0.002 $nm^{-1}$ and 0.019 ± 0.002 $nm^{-1}$ to 0.017 ± 0.002 $nm^{-1}$, respectively (Figure 4c). Bangka stations reported a fluctuation in the value of $S_{350\text{-}400}$, ranging from 0.016 ± 0.003 $nm^{-1}$ to 0.018 ± 0.002 $nm^{-1}$. $S_{350\text{-}400}$ values between 0.015 ± 0.005 $nm^{-1}$ and 0.017 ± 0.003 $nm^{-1}$ reveal a declining pattern in river mouth and coastal water (Figure 4c). The spatial distribution of $S_{350\text{-}400}$ showed statistically opposite pattern from $S_{275\text{-}295}$ where the $S_{350\text{-}400}$ decreased from rivers to the coastal area ($p < 0.05$).

During the SIM, the monsoonal means of $S_{350\text{-}400}$ fluctuated, especially from Station 1 to Station 7 (Darau), as shown in Figure 4d. During FIM, a sharp drop in the S350-500 value (0.006 $nm^{-1}$) was seen at Station 17, which is located near the coast (Figure 4d). The $S_{350\text{-}400}$ of monsoonal variations during the study period were 0.016 $nm^{-1}$ to 0.019 $nm^{-1}$ (SWM), 0.015 $nm^{-1}$ to 0.018 $nm^{-1}$ (NEM), 0.006 $nm^{-1}$ to 0.019 $nm^{-1}$ (FIM), and 0.010 $nm^{-1}$ to 0.020 $nm^{-1}$ (SIM) (Figure 4d). In general, the monsoonal distribution of $S_{350\text{-}400}$ showed statistically significant differences between monsoons ($p < 0.05$).

Figure 4e displays the spatial mean of $S_{300\text{-}600}$ at the Darau, Inanam, and Bangka stations, which showed a consistent trend ranging from 0.014 ± 0.002 $nm^{-1}$ to 0.016 ± 0.004 $nm^{-1}$. $S_{300\text{-}600}$ value drops from the river mouth (Station 15 and 16) to coastal area stations (Station 17, 18, and 19), with a range of 0.012 ± 0.003 $nm^{-1}$ to 0.013 ± 0.004 $nm^{-1}$ (Figure 4e). However, the $S_{300\text{-}600}$ did not show any significant pattern between sampling points during the 14-months of the study period ($p > 0.05$). As shown in Figure 4f, the monsoonal pattern of $S_{300\text{-}600}$ revealed an up and down trend in SIM at Darau stations with the value of 0.007 $nm^{-1}$ (Station 4) and 0.017 $nm^{-1}$ (Station 3). There were very slight monsoonal changes in $S_{300\text{-}600,}$ ranging from 0.012 to 0.015 (SWM), 0.012 to 0.018 (NEM), and 0.009 to 0.015 (FIM) (Figure 4f). Statistically, the monsoonal distribution of $S_{300\text{-}600}$ showed significant differences between monsoons throughout the study period ($p < 0.05$).

The spatial means and their standard deviations of spectral ratio ($S_R$) peaked at Station 7 (Darau) and Station 17 (coastal water) with values of 1.22 ± 0.61 and 1.40 ± 0.68, respectively, as plotted in Figure 4g. Furthermore, an increased pattern of $S_R$ values at the Darau stations (0.86 ± 0.13 to 1.22 ± 0.61) and Inanam River (0.81 ± 0.16 to 1.01 ± 0.45) was recorded during the study period (Figure 4g). In contrast, Station 17, 18, and 19 located at the coastal water indicated a declining slope with 1.60 ± 0.48 to 1.13 ± 0.31 (Figure 4g). The spatial distribution of $S_R$ showed statistically significant differences between sampling points during the study period ($p < 0.05$).

Overall, the monsoonal distribution of SR showed statistically significant differences between monsoons ($p < 0.05$). In FIM, the most significant monsoonal mean of $S_R$ was observed at Station 17, located near the coast, with a value of 3.46, as shown in Figure 4h. $S_R$ readings ranged from 0.81 to 1.51 in Darau stations during SIM and from 0.70 to 1.29 in Bangka stations (Figure 4h). The monsoonal mean of $S_R$ during NEM and SWM at the study area, on the other hand, had a constant trend, ranging from 0.79 (Station 1) to 1.44 (Station 7) at Darau Station and 0.81 (Station 12 at Inanam River) to 1.34 (Station 19 at the coastal water) respectively (Figure 4h).

### 3.4. Relationship between salinity with $a_{CDOM}(440)$, $S_{275\text{-}295}$, $S_{350\text{-}400}$, and $S_R$

The regression analysis between $a_{CDOM}(440)$ and salinity during 14-month observation in the study period showed a weak negative relationship with R-value of −0.322 ($p = 0.000$, $n = 254$) as illustrated in Figure 5a. Therefore, the inter-seasonal monsoon attributed the highest correlation between $a_{CDOM}(440)$ and salinity with R-value of −0.73 ($p = 0.000$, $n = 31$) during FIM, −0.59 ($p = 0.000$, $n = 37$) in SIM monsoon (Figure 5a). A moderate correlation between $S_{275\text{-}295}$ and salinity with R-value of 0.55 ($p = 0.00$, $n = 252$) as plotted in Figure 5b. The monsoonal trends of $S_{275\text{-}295}$ and salinity correlation showed more a less the same in observed monsoons with R-value of 0.60 ($p = 0.00$, $n = 30$) (FIM), 0.51 ($p = 0.00$, $n = 71$) (NEM), and 0.44 ($p = 0.006$, $n = 37$) (SIM). However, $S_{275\text{-}295}$ and salinity correlation during SWM was relatively higher compared to another observed monsoon with R-value of 0.66($p = 0.00$, $n = 111$) (Figure 5b).

There is a low inverse correlation between $S_{350\text{-}400}$ and salinity with R-value of 0.33 ($p = 0.00$, $n = 254$) during 14-month observation in the study period as shown in Figure 5c. The lowest correlation between $S_{350\text{-}400}$ and salinity was in NEM monsoon (R-value = −0.11, $p = 0.36$, $n = 71$), while R-value of $S_{350\text{-}400}$ and salinity is relatively larger ($r = -0.48$, $p = 0.005$, $n = 31$) in FIM monsoon (Figure 5c). The relationship between the ratio of spectra slope (SR) and salinity indicate a lenient correlation at the study area with R-value of 0.53 ($p = 0.00$, $n = 253$) based on the 14-month observation (Figure 5d). Moreover, SWM depicts a relatively good correlation with R-value of 0.67 ($p = 0.000$, $n = 111$) (Figure 5d). On the other hand, r- value of 0.39 ($p = 0.001$, $n = 71$) was recorded in NEM monsoon, which the lowest magnitude compared to other observed monsoons (Figure 5d). As for the $S_{300\text{-}600}$, no significant correlations were observed throughout the 14-month observation and during each monsoon.

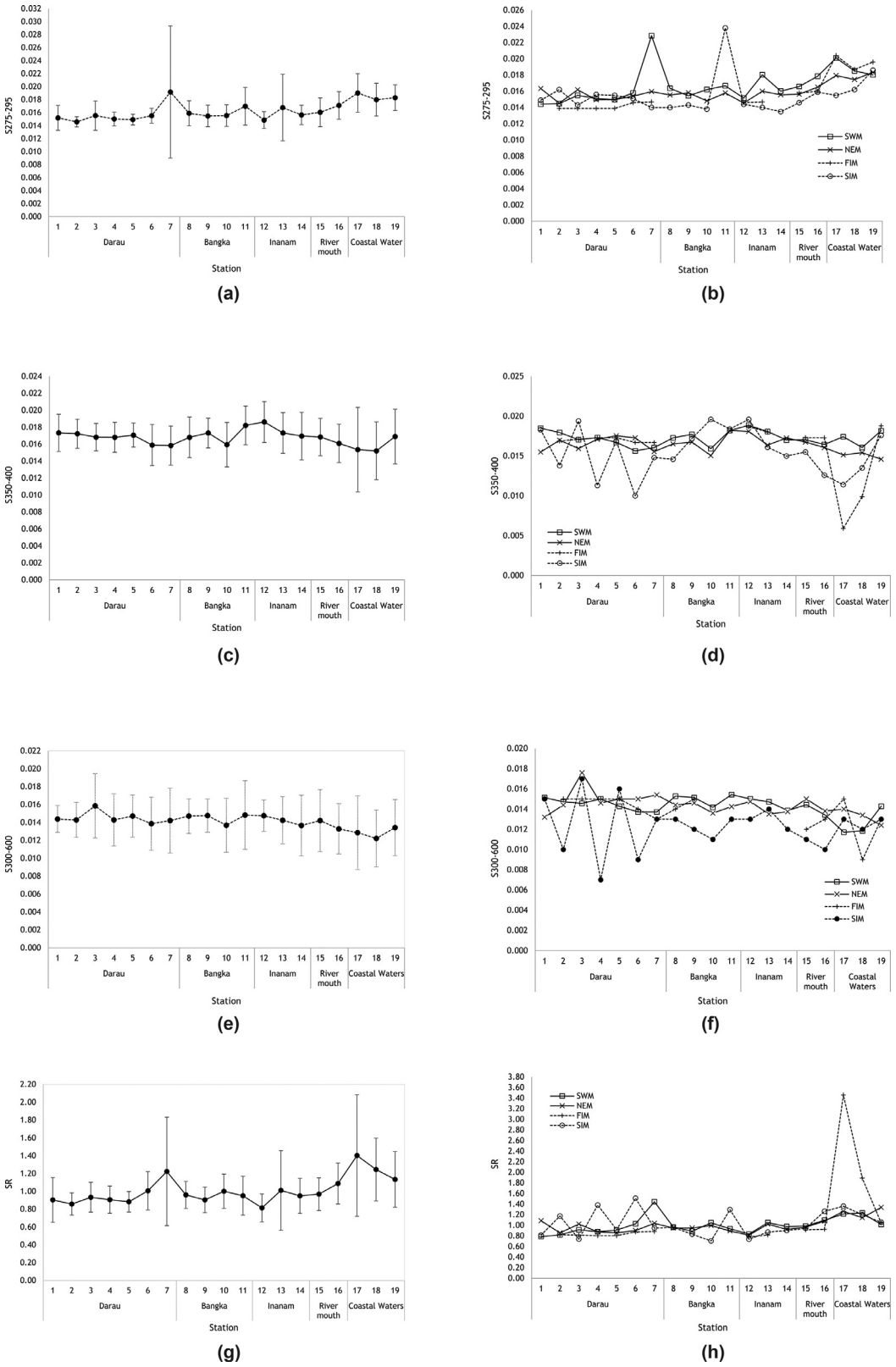


**Figure 4** The temporal and monsoonal mean of spectral slopes: $S_{275\text{-}295}$, $S_{350\text{-}440}$, and $S_R$ at each station during 14-month observation in the study area.

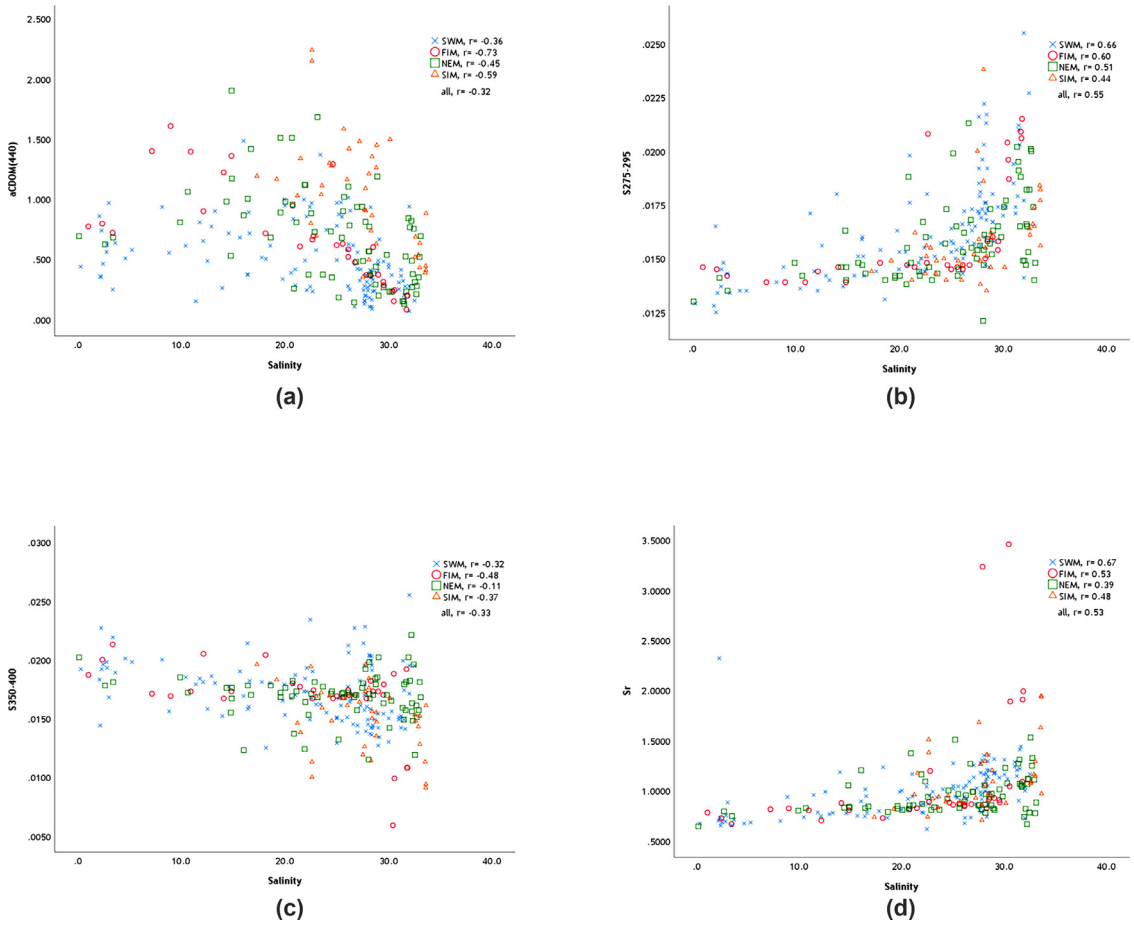


**Figure 5** Scatter plots of regression correlation (r) between salinity and a) CDOM absorption coefficient at 440 [aCDOM(440)], b) $S_{275\text{-}295}$, c) $S_{350\text{-}440}$ and d) the ratio of spectral slope (SR) for the 14-month observation at the study area. The r-value stated in the legend of the plot.

### 3.5. Relationship between $S_{275\text{-}295}$, $S_{350\text{-}440}$, and $S_R$ with $a_{CDOM}(440)$

A moderate correlation between $S_{275\text{-}295}$ and $a_{CDOM}(440)$ was observed in the study area based on the 14-month observation with R-value of −0.57 (($p = 0.000$, $n = 252$) as illustrated in Figure 6a. For the monsoonal pattern of relationship of $S_{275\text{-}295}$ and $a_{CDOM}(440)$, SWM, FIM and NEM depict a relatively strong correlation with R-values of −0.65 ($p = 0.000$, $n = 111$), −0.67 ($p = 0.000$, $n = 30$) and −0.70 ($p = 0.000$, $n = 71$) respectively (Figure 6a). A lenient $S_{275\text{-}295}$ and $a_{CDOM}(440)$ correlations were recorded during SIM with R-values of 0.37 ($p = 0.023$, $n = 37$) (Figure 6a). There is a very weak relationship between $S_{350\text{-}400}$ and $a_{CDOM}(440)$ in this study as indicated by the small R-value of 0.05 ($p = 0.456$, $n = 254$), which is plotted in Figure 6b. Of all observed monsoons were reported smaller R-values; SWM (0.11, $p = 0.244$, $n = 112$), NEM (0.19, $p = 0.113$, $n = 71$), and SIM (0.11, $p = 0.532$, $n = 37$), FIM monsoon attributed a relatively larger R-value (0.33, $p = 0.068$, $n = 31$) compared to other monsoons (Figure 6b). The R-value of regression correlation between $S_R$ and $a_{CDOM}(440)$ in the study area is −0.30 ($p = 0.000$, n= 253) as shown in Figure 6c. There are two monsoonal patterns of $S_R$ and $a_{CDOM}(440)$ during the study period, where NEM (−0.56, $p = 0.000$, $n = 71$) and FIM (−0.50, $p = 0.004$, $n = 31$) monsoon a moderate correlation (Figure 6c). Meanwhile, SWM and SIM monsoon attributed a weak relationship between $S_R$ and $a_{CDOM}(440)$ with R-value of (−0.35, $p = 0.000$, $n = 112$) and (−0.27, $p = 0.103$, $n = 37$) respectively (Figure 6c).

## 4. Discussion

### 4.1. Dynamics of $a_{CDOM}(440)$

The spatial mean $a_{CDOM}(440)$ in the study area, ranging from 0.29 ± 0.19 $m^{-1}$ to 1.05 ± 0.39 $m^{-1}$, indicated a decreasing pattern towards the coastal water. The spatial declining trends of $a_{CDOM}(440)$ in the study area are predictable as a signature of CDOM distribution in coastal waters. Several studies recorded a spatial gradient of $a_{CDOM}(440)$ in coastal waters with a range of 2.5 to 7.6 $m^{-1}$ in the mangrove area in the Indian Suburbans (Sanyal et al., 2020). The $a_{CDOM}(440)$ of 0.063 to 0.35 $m^{-1}$ was recorded worldwide in the natural water bodies (Nima et al., 2019). In addition, $a_{CDOM}(440)$ of 0.35 $m^{-1}$ to >50 $m^{-1}$ at peatland-draining rivers and coastal waters of Sarawak, Borneo (Martin et al., 2018). The $a_{CDOM}(440)$ at the continental shelf of the northern Bay of Bengal ranged from 0.1002 $m^{-1}$ and 0.6631 $m^{-1}$

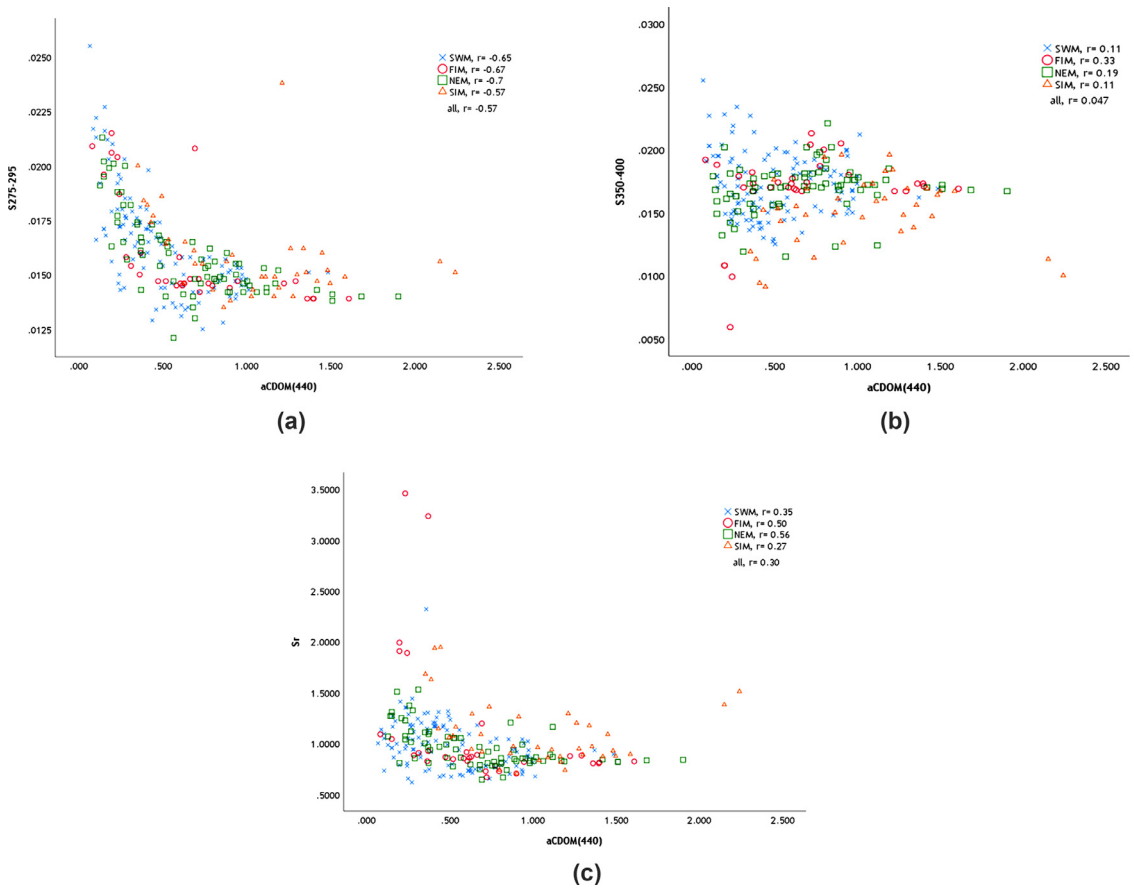


**Figure 6** Scatter plots of regression correlation (r) between CDOM absorption coefficient at 440 [aCDOM(440)] and a) $S_{275\text{-}295}$, b) $S_{350\text{-}440}$ and c) the ratio of spectral slope (SR) for the 14-month observation at the study area. The r-value stated in the legend of the plot.

(Das et al., 2017); and 0.66 to 3.82 $m^{-1}$ at microtidal estuary in south-western Australia (Kostoglidis et al., 2005).

Higher $a_{CDOM}(440)$ upstream in the study area might be associated with a strong influence of terrestrial organic matter and humic substances carried by freshwater input (aligned with the lowest salinity). Many studies have shown that terrigenous DOM is the primary source of natural CDOM in coastal and nearshore areas, where freshwater runoff mixes with seawater (Coble, 2007; Granskog et al., 2007; Li et al., 2014; Stedmon et al., 2011). In addition, as a mangrove area fringes the study area, the possible source of higher CDOM concentration upstream was likely mangrove influenced water flushing organic matter from the decomposition of mangrove forests. Several studies have revealed that mangrove leaf litter can produce CDOM more rapidly than other local indigenous CDOM sources (Das et al., 2017; Sanyal et al., 2020; Shank and Evans, 2011). The decreasing pattern of $a_{CDOM}(440)$ from the upstream to coastal areas in the study area could be attributed to several possible factors, such as (i) the mixing of CDOM-rich riverine water with CDOM-poor coastal water (del Vecchio and Blough, 2004; Gonsior et al., 2008), (ii) enhancing the photodegradation of chromophores present in riverine CDOM after they reach the coastal regions (Blough and del Vecchio, 2002; del Vecchio and Blough, 2004; Osburn et al., 2009), (iii) microbial degradation of the autochthonous fraction that is the central part of CDOM in marine waters (Boyd and Osburn, 2004; Broman et al., 2019; Winter et al., 2007), as well as (iv) flocculation and precipitation of riverine CDOM due to increased salinity (Blough et al., 1993; Guo et al.,2007; Sholkovitz, 1976).

The monsoonal variations of $a_{CDOM}(440)$ were relatively higher during the SIM (April 2019) and FIM (October 2018) monsoons with varied from 0.49 to 2.24 $m^{-1}$ and 0.15 to 1.61 $m^{-1}$, respectively. However, the former indicated a fluctuated pattern in Darau the stations. Higher $a_{CDOM}(440)$ during the inter-seasonal monsoons (SIM and FIM) may be attributable to the fact that east coast Malaysian water is well-mixed, with water temperature distributed evenly throughout the water body (Mohd-Akhir et al., 2014). On the other hand, the current circulation may impact it by allowing stratification or stimulating mixing during inter-seasonal monsoon (Mohd-Akhir et al., 2014). In the continental shelf of the northern Bay of Bengal, seasonal mean $a_{CDOM}(440)$ showed a significant difference in magnitudes during the three seasons, with lower values of 0.1200 to 0.0327 $m^{-1}$ during the pre-monsoon (February to May), increasing to 0.3064 0.1595 $m^{-1}$ during the monsoon season (June to September), and 0.1621 to 0.0790 $m^{-1}$ during the post-monsoon (October to January) (Das et al., 2017). Li et al. (2017) also found a seasonal variability of $a_{CDOM}(400)$, higher in Yinma River, China. The temporal variability is due

to strong riverine influence during specific monsoon or season (Das et al., 2016, Li et al., 2017).

### 4.2. Spatio-temporal trends of spectral slopes

There was a slight spatial variation of spectral slope of $S_{275\text{-}295}$ between stations during the study period ranging from 0.015 to 0.019 $nm^{-1}$ in the study area. $S_{275\text{-}295}$ showed an increment of 0.004 $nm^{-1}$ from the upstream of Darau River, located 5.1 km from the river mouth (station 16). The monsoon patterns of $S_{275\text{-}295}$ indicated relatively higher spatial variability during SWM (June to September 2018, June to July 2019) and SIM (April 2019) monsoon with an increment of 0.009 $nm^{-1}$. In contrast, NEM (November 2018 to March 2019) indicated a smaller spatial gradient of $S_{275\text{-}295}$ with an increment of 0.003 $nm^{-1}$. In other studies, in peatland draining rivers and coastal waters of Sarawak, Borneo, $S_{275\text{-}295}$ values ranged from 0.0102 to 0.0144 $nm^{-1}$ (Martin et al., 2018), which was a little lower compared to the study area. However, there was no clear seasonality of $S_{275\text{-}295}$ in peatland draining rivers and coastal waters of Sarawak, Borneo. The distance of observed rivers ranged between 15 to 550 km (Martin et al., 2018), in contrast with the monsoonal variability in the study area. In a river and mangrove-dominated estuaries in Indian Sundarbans, a slight spatial difference of $S_{275\text{-}295}$ was recorded with 0.002 to 0.007 $nm^{-1}$ (Sanyal et al., 2020), which is lower compared to this study. The spatial difference of $S_{275\text{-}295}$ in this study compared to Sanyal et al. (2020) is due to the morphology of the estuary in Indian Sundarbans, which have a wider inlet than the study area. While the $S_{275\text{-}295}$ varies with 0.0130 $nm^{-1}$ to 0.0361 $nm^{-1}$ were recorded from the Elizabeth River towards Chesapeake Bay estuary with increasing spatial gradient, as it receives substantial input of CDOM-rich water from the Great Dismal Swamp canal system (Helms et al., 2008).

The small range of spatial distribution of $S_{350\text{-}400}$ in the study area was 0.015 $nm^{-1}$ to 0.019 $nm^{-1}$, with higher at the upstream and lower at the coastal water of the study area. The monsoonal pattern indicated that inter-seasonal monsoon had more considerable spatial differences with 0.010 $nm^{-1}$ and 0.013 $nm^{-1}$ during FIM and SIM. These values were about three and four times the increment of $S_{350\text{-}400}$ during SWM and NEM monsoon, which had 0.003 of $S_{350\text{-}400}$ declining pattern from the upstream to coastal water. In another study, a small variability of $S_{350\text{-}400}$ was found in the Elizabeth River towards Chesapeake Bay estuary with 0.0104 to 0.0187 (Helms et al., 2008), which is also within the range of this study area. The shallower slope of $S_{350\text{-}400}$ is probably due to a decrease in molecular weight, which diminishes the potential for intramolecular charge transfer interaction (Helms et al., 2008).

A decreased pattern spatial variation of $S_{300\text{-}600}$ with a range of 0.012 to 0.016 $nm^{-1}$ was observed apparently at the river mouth towards coastal water in the study area. The other stations were mainly recorded with a consistent mean $S_{300\text{-}600}$ with 0.014 $nm^{-1}$. Similar to the monsoonal trend of $S_{350\text{-}400}$ in the study area, $S_{300\text{-}600}$ had a relatively more significant spatial variation during the inter-seasonal monsoons: SIM (0.007 to 0.017 $nm^{-1}$), and FIM (0.009 to 0.015 $nm^{-1}$) with 0.010 $nm^{-1}$ and 0.09 $nm^{-1}$ spatial differences, respectively. Whilst, the spatial variations of $S_{300\text{-}600}$ were lower during SWM, with a gap of 0.003 and 0.006 in the NEM monsoon. In the Arctic Ocean, $S_{300\text{-}600}$ varies between 0.008 $nm^{-1}$ and 0.047 $nm^{-1}$. Still, in the Eurasian part of the Arctic Ocean and the Greenland Sea, the values are lower, 0.015—0.021 $nm^{-1}$ (Stedmon et al., 2011) and 0.016—0.020 $nm^{-1}$ (Stedmon and Markager, 2001), respectively. Moreover, the $S_{300\text{-}600}$ in the Eurasian part of the Arctic Ocean and the Greenland Sea is within the range with corresponding values for our study area. Past studies have shown strong relationships between *a*CDOM and SCDOM along transects from lower salinity coastal waters to higher salinity offshore waters, where the range in *a*CDOM($\lambda$) typically varies by orders of magnitude (Kowalczuk et al., 2006; Pavlov et al., 2016; Stedmon and Markager, 2005), which was a contrast with the values in our study area. However, the value of $S_{300\text{-}600}$ (SCDOM) in our study area was in agreement with a study in the Arctic Ocean that found that CDOM absorption and SCDOM do not relate well between marine and terrestrially derived CDOM pools (Granskog, 2012). In addition, a study by Astoreca et al. (2009) found S increases with increasing salinity and decreasing aCDOM as a result of the alteration of terrestrial CDOM (Blough and Del Vecchio, 2002 and references therein, S: 0.018—0.030 $nm^{-1}$ for salinities 30—35).

The spatial patterns of $S_R$ and $S_{275\text{-}295}$ in the study area had an identical trend, higher in the coastal water and lowered numbers upstream. The spatial range of $S_{300\text{-}600}$ was 0.81 to 1.40. The SIM and FIM, which are inter-seasonal monsoons, showed higher values of $S_R$ with monsoonal differences of 2.68 and 0.81, respectively, compared to $S_{300\text{-}600}$ in SWM (0.65) and NEM (0.53) monsoons. The $S_R$ values observed upstream of the river mouth were typical of terrestrially dominated samples (0.81), while the $S_R$ values observed in coastal areas were specific to marine-dominated samples (1.40). We observed an increasing trend in $S_R$ from upstream (terrestrial-dominated) to coastal areas (marine-dominated) sources. Despite most of the stations that are located in the Darau, Inanam, and Bangka-Bangka rivers had $S_R$ values that were less than 1. Hence, CDOM in these stations is a terrestrial-dominated source. On the other hand, as the value of $S_R$ is more than one at the river mouth to coastal waters, it indicates that the CDOM is a marine-dominated source. The increasing importance of $S_R$ from upstream toward the coastal area may indicate a compositional change in the DOM pool and a shift from high molecular weight to low molecular weight (Helms et al., 2008; Nima et al., 2019; Xie et al., 2012).

### 4.3. Relationship of $a_{CDOM}(440)$, spectral slopes $S_{275\text{-}295}$, $S_{350\text{-}440}$, and $S_R$ and salinity

In the study area, a higher value of $a_{CDOM}(440)$ corresponded with lower values of salinity at upstream stations of the river, which could be related to revealing that the higher CDOM concentration of terrigenous origin contained chromophores of larger molecular size and weight, linked to lignin derivatives which can be explained by the abundance of mangrove forests distributed along the river. The $a_{CDOM}(440)$ variability showed a strong inverse correlation with salinity, which indicated the conservative behaviour of CDOM in the study area as observed in other estuarine

systems (Blough and Del Vecchio, 2002; Bowers and Brett, 2008; Chen et al., 2007; Das et al., 2017; Del Vecchio and Blough, 2004; Nima et al., 2019; Twardowski and Donaghay, 2001). A strong correlation between $a_{CDOM}(440)$ and salinity during inter-seasonal monsoons probably can be due to the strong riverine influence (Das et al., 2017; Li et al., 2017; Nima et al., 2019) which could be associated with transition monsoon in the study area.

There was a moderate correlation between spectral slopes of $S_{275\text{-}295}$ and salinity, greater for the NEM monsoon (R-value = 0.5, p = 0.00, n = 71) in the study area. The trend of $S_{275\text{-}295}$ was inversely proportional to $S_{350\text{-}400}$ in the study area, in which the former had an increasing pattern from the upstream towards coastal water and vice versa for the latter. Nevertheless, the correlation between $S_{350\text{-}400}$ and salinity was relatively greater during the FIM monsoon (r-value = 0.48, p = 0.005, n= 31). As $S_{350\text{-}400}$ was greater than $S_{275\text{-}295}$ upstream of the river mouth, terrestrially dominated CDOM prevails (Helms et al., 2008). In contrast, as $S_{275-295}$ was greater than $S_{350\text{-}500}$ in coastal stations, marine-dominated CDOM prevails in coastal waters, composed of a smaller molecular size and weight.

$S_{300\text{-}600}$ was relatively constant over the same salinity range and $a_{CDOM}(440)$ in our study area. In addition, there was no statistical difference in $S_{300\text{-}600}$ test during the study period due to the small coverage of the study area. As a result, the relationship between $S_{300\text{-}600}$ versus salinity and $a_{CDOM}(440)$ was not executed. Upstream to the river mouth, $S_{300\text{-}600}$ values were constant ($\sim$0.014 $nm^{-1}$), indicating a continuous influence of terrestrial inputs to the region throughout the sampling period (Figure 4e). However, $S_{300\text{-}600}$ values were more variable near the river mouth areas and coastal areas in the study area, presumably due to different CDOM pools entering the system in these areas and could be related to renewed high freshwater inflow after rain (Stedmon et al., 2015).

The spatial distribution of $S_{275\text{-}295}$ and $S_R$ are linear correlated in the study area. As a result, the relationship between $S_R$ and salinity in response to monsoonal variability is identical correlated to the greater degree during SWM (r-value = 0.66, p = 0.000) for the former, and (r-value = 0.67, p = 0.000) for the latter. Generally, $S_R$ increases with salinity and may be linked to photobleaching processes that usually occur in coastal areas or on open seas (Granskog, 2012; Helms et al., 2008; Lei et al., 2019; Nima et al., 2019). In high salinity regions, higher $S_R$ values and low $a_{CDOM}(440)$ values are indicative of photobleaching of decomposed humic substances, which produced more low-molecular-weight fractions as exposed to solar irradiance in coastal areas (Helms et al., 2008; Nima et al., 2019). Photodegradation of CDOM can shift the absorption spectrum by breaking up large humic complexes and thus decreasing the number and size of the low-energy chromophores associated with large humic complexes (Helms et al., 2008; Nima et al., 2019).

The correlation between $S_{275\text{-}295}$ and $a_{CDOM}(440)$ in the study area during the study period indicated a good relationship with an R-value of 0.51, which is stronger correlated compared to other spectral wavelengths. This condition agrees with Grunert et al. (2018), which also found that $S_{275\text{-}295}$ is better correlated with $a_{CDOM}(440)$ than other spectral wavelengths because of lignin or lignin derivatives. According to Helms et al. (2008), both $S_{275\text{-}295}$ and $S_R$ were inversely correlated to the molecular weight of CDOM. Both $S_{275\text{-}295}$, $S_{350\text{-}400}$, and $S_R$ showed a significant inverse relationship with $a_{CDOM}(440)$ and salinity in the study, which agrees with Nima et al. (2019) and Li et al. (2017).

## 5. Conclusions

Monsoonal variation of $a_{CDOM}(440)$ in the study area with higher concentration was associated with a steeper slope at 300 to 350 nm during inter-seasonal monsoon. $S_{300\text{-}600}$ indicates a linear relationship between $a_{CDOM}(440)$, these unconventional results in coastal water might be due to the limited coverage of the study site.

The upstream of the Likas estuary indicated terrestrial-dominated sources of CDOM. However, the CDOM at the river mouth to coastal water showed a marine-dominated source. Therefore, our observations during the study period indicate that the monsoonal variation could alter the source of CDOM in the study area.

## Acknowledgements

This study was funded by Universiti Malaysia Sabah: (SLB0158-2017 and UMSGreat 2018/2019 grants) and by the Ministry of Higher Education of Malaysia FRGS Grant: (FRGS/1/2019/STG03/UMS/02/2). The staff from Borneo Marine Research Institute (BMRI) UMS, especially boathouse crews and laboratory assistants, are thanked for their assistance during field and laboratory assistance.

## References

Andrew, A., Del Vecchio, R., Subramaniam, A., Blough, N., 2013. Chromophoric dissolved organic matter (CDOM) in the Equatorial Atlantic Ocean: Optical properties related to CDOM structure and source. Mar. Chem. 148, 33–43. https://doi.org/10.1016/j.marchem.2012.11.001

Astoreca, R., Rousseau, V., Lancelot, C., 2009. Coloured dissolved organic matter (CDOM) in Southern North Sea waters: Optical characterisation and possible origin. Estuar. Coast. Shelf Sci. 85 (4), 633–640. https://doi.org/10.1016/j.ecss.2009.10.010

Blough, N., Zafiriou, O., Bonilla, J., 1993. Optical absorption spectra of waters from the Orinoco River outflow: terrestrial input of colored organic matter to the Caribbean. J. Geophys. Res. 98 (C2), 2271–2278. https://doi.org/10.1029/92JC02763

Blough, N.V., Green, S.A., 1995. Spectroscopic characterisation and remote sensing of non-living organic matter. In: Zepp, R.G., Sontag, C. (Eds.), The Role of Non-living Organic Matter in the Earth's Carbon Cycle. John Wiley & Sons, 23–45.

Blough, N.V., Del Vecchio, R., 2002. Chromophoric DOM in the Coastal Environment. In: Hansell, D.A., Carlson, C.A. (Eds.), Biogeochemistry of Marine Dissolved Organic Matter. Academic Press, California, 509–546.

Bowers, D.G., Brett, H.L., 2008. The relationship between CDOM and salinity in estuaries: an analytical and graphical solution. J. Mar. Syst. 73 (1–2), 1–7. https://doi.org/10.1016/j.jmarsys.2007.07.001

Bowen, J.C., Clark, C.D., Keller, J.K., De Bruyn, W.J., 2017. Optical properties of chromophoric dissolved organic matter (CDOM) in surface and pore waters adjacent to an oil well in a south-

ern California salt marsh. Mar. Pollut. Bull. 114 (1), 157—168. https://doi.org/10.1016/j.marpolbul.2016.08.071

Brandão, L.P.M., Brighenti, L.S., Staehr, P.A., Asmala, E., Massicotte, P., Tonetta, D., Barbosa, F.A.R., Pujoni, D., Bezerra-Neto, J.F., 2018. Distinctive effects of allochthonous and autochthonous organic matter on CDOM spectra in a tropical lake. Biogeosciences 15 (9), 2931—2943. https://doi.org/10.5194/bg-15-2931-2018

Bricaud, A., Morel, A., Prieur, L., 1981. Absorption by dissolved organic matter of the sea (yellow substance) in the UV and visible domains. Limnol. Oceanogr. 26 (1), 45—53. https://doi.org/10.4319/lo.1981.26.1.0043

Broman, E., Asmala, E., Carstensen, J., Pinhassi, J., Dopson, M., 2019. Distinct coastal microbiome populations are associated with autochthonous- and allochthonous-like Dissolved Organic Matter. Front. Microbiol. 10, 2579. https://doi.org/10.3389/fmicb.2019.02579

Boyd, T.J., Osburn, C.L., 2004. Changes in CDOM fluorescence from allochthonous and autochthonous sources during tidal mixing and bacterial degradation in two coastal estuaries. Mar. Chem. 89 (1—4), 189—210. https://doi.org/10.1016/j.marchem.2004.02.012

Chen, Z., Hu, C., Conmy, R.N., Muller-Karger, F., Swarzenski, P., 2007. Colored dissolved organic matter in Tampa Bay. Florida. Mar. Chem. 104 (1—2), 98—109. https://doi.org/10.1016/j.marchem.2006.12.007

Coble, P.G., 2007. Marine Optical Biogeochemistry: The Chemistry of Ocean Color. Chem. Rev. 107 (2), 402—418. https://doi.org/10.1021/cr050350

Coble, P.G., Nelson, N., 2009. Optical Analysis of Chromophoric Dissolved Organic Matter. In: Wurl, O. (Ed.), Practical guidelines for the Analysis of Seawater. CRC Press, Boca Raton, 18—27.

Das, S., Hazra, S., Lotlikar, A.A., Das, I., Giri, S., Chanda, A., Akhand, A., Maity, S., Kumar, T.S., 2016. Delineating the relationship between chromophoric dissolved organic matter (CDOM) variability and biogeochemical parameters in a shallow continental shelf. Egypt. J. Aquat. Res. 42 (3), 241—248. https://doi.org/10.1016/j.ejar.2016.08.001

Das, S., Das, I., Giri, S., Chanda, A., Maity, S., Lotliker, A.A., Kumar, T.S., Akhand, A., Hazra, S., 2017. Chromophoric dissolved organic matter (CDOM) variability over the continental shelf of the northern Bay of Bengal. Oceanologia 59 (3), 271—282. https://doi.org/10.1016/j.oceano.2017.03.002

Del Vecchio, R., Blough, N.V., 2004. On the Origin of the Optical Properties of Humic Substances. Environ. Sci. Technol. 38 (14), 3885—3891. https://doi.org/10.1021/es049912h

Ferrari, G.M., 2000. The relationship between chromophoric dissolved organic matter and dissolved organic carbon in the European Atlantic coastal area and in the West Mediterranean Sea (Gulf of Lions). Mar. Chem. 70 (4), 339—357. https://doi.org/10.1016/S0304-4203(00)00036-0

Gonsior, M., Peake, B., Jaffe, R., Heather, Y., Dickens, A., Kowalczuk, P., 2008. Spectral characterisation of chromophoric dissolved organic matter (CDOM) in a fjord (Doubtful Sound, New Zealand). Aquat. Sci. 70, 397—409. https://doi.org/10.1007/s00027-008-8067-4

Granskog, M.A., Macdonald, R.W., Mundy, C.J., Barber, D.G., 2007. Distribution, characteristics and potential impacts of Chromophoric dissolved organic matter (CDOM) in Hudson Strait and Hudson Bay. Canada. Cont. Shelf Res. 27 (15), 2032—2050. https://doi.org/10.1016/j.csr.2007.05.00

Granskog, M.A., 2012. Changes in spectral slopes of colored dissolved organic matter absorption with mixing and removal in a terrestrially dominated marine system (Hudson Bay, Canada). Mar. Chem. 134—135, 10—17. https://doi.org/10.1016/j.marchem.2012.02.008

Green, Sarah A., Blough, N.V., 1994. Optical absorption and fluorescence properties of chromophoric dissolved organic matter in natural waters. Limnol. Oceanogr. 39 (8), 1903—1916. https://doi.org/10.4319/lo.1994.39.8.1903

Grunert, B.K., Mouw, C.B., Ciochetto, A.B., 2018. Characterising CDOM Spectral Variability across Diverse Regions and Spectral Ranges. Global Biogeochem. Cy. 32 (1), 57—77. https://doi.org/10.1002/2017GB005756

Guèguen, C., Guo, L., Tanaka, N., 2005. Distributions and characteristics of colored dissolved organic matter in the Western Arctic Ocean. Cont. Shelf Res. 25, 1195—1207. https://doi.org/10.1016/j.csr.2005.01.005

Guo, W., Stedmon, C.A., Han, Y., Wu, F., Yu, X., Hu, M., 2007. The conservative and non-conservative behavior of chromophoric dissolved organic matter in Chinese estuarine waters. Mar. Chem. 107 (3), 357—366. https://doi.org/10.1016/j.marchem.2007.03.006

Helms, J.R., Stubbins, A., Ritchie, J.D., Minor, E.C., Kieber, D.J., Mopper, K., 2008. Absorption spectral slopes and spectral ratios as indicators of molecular weight, source and photobleaching of chromophoric dissolved organic matter. Limnol. Oceanogr. 53 (3), 955—969. https://doi.org/10.4319/lo.2008.53.3.0955

Hickman, A.E., Dutkiewicz, S., Williams, R.G., Follows, M.J., 2010. Modelling the effects of chromatic adaptation on phytoplankton community structure in the oligotrophic ocean. Mar. Ecol. Prog. Ser. 406, 1—17. https://doi.org/10.3354/MEPS08588

Kim, G.E., Gnanadesikan, A., Pradal, M.A., 2016. Increased Surface Ocean Heating by Colored Detrital Matter (CDM) Linked to Greater Northern Hemisphere Ice Formation in the GFDL CM2Mc ESM. J. Clim. 29 (24), 9063—9076. https://doi.org/10.1175/JCLI-D-16-0053

Kirk, J.T.O., 1994. Characteristics of the light field in highly turbid waters: a Monte Carlo study. Limnol. Oceanogr. 39 (3), 702—706. https://doi.org/10.4319/lo.1994.39.3.0702

Kostoglidis, A., Pattiaratchi, C.B., Hamilton, D.P., 2005. CDOM and its contribution to the underwater light climate of a shallow, microtidal estuary in south-western Australia. Estuar. Coaat. Shelf Sci. 63 (4), 469—477. https://doi.org/10.1016/j.ecss.2004.11.016

Kowalczuk, P., Stedmon, C.A., Markager, S., 2006. Modeling absorption by CDOM in the Baltic Sea from season, salinity and chlorophyll. Mar. Chem. 101, 1—11.

Lei, X., Pan, J., Devlin, A.T., 2019. Characteristics of Absorption Spectra of Chromophoric Dissolved Organic Matter in the Pearl River Estuary in Spring. Remote Sens. 11 (13), 1533. https://doi.org/10.3390/rs11131533

Li, G., Liu, J., Ma, Y., Zhao, R., Hu, S., Li, Y., Wei, H., Xie, H., 2014. Distribution and spectral characteristics of chromophoric dissolved organic matter in a coastal bay in northern China. J. Environ. Sci. (China) 26 (8), 1585—1595. https://doi.org/10.1016/j.jes.2014.05.025

Li, S., Zhang, J., Guo, E., Zhang, F., Ma, Q., Mu, G., 2017. Dynamics and ecological risk assessment of chromophoric dissolved organic matter in the Yinma River Watershed: Rivers, reservoirs, and urban waters. Environ. Res. 158, 245—254. https://doi.org/10.1016/j.envres.2017.06.020

Martin, P., Cherukuru, N., Tan, A.S.Y., Sanwlani, N., Mujahid, A., Müller, M., 2018. Distribution and cycling of terrigenous dissolved organic carbon in peatland-draining rivers and coastal waters of Sarawak. Borneo. Biogeosciences 15, 6847—6865. https://doi.org/10.5194/bg-15-6847-2018

Menon, H.B., Sangekar, N.P., Lotliker, A.A., Vethamony, P., 2011. Dynamics of chromophoric dissolved organic matter in Mandovi and Zuari estuaries — A study through in situ and satellite data. ISPRS J. Photogramm. Remote Sens. 66 (4), 545—552. https://doi.org/10.1016/j.isprsjprs.2011.02.011

Minu, P., Souda, V.P., Baliarsingh, S.K., Dwivedi, R.M., Ali, Y., Ashraf, P.M., 2020. Assessing temporal variation of coloured dissolved organic matter in the coastal waters of South East-

ern Arabian Sea. Acta Oceanologica Sinica 39 (1), 102—109. https://doi.org/10.1007/s13131-020-1534-z

Mohd Akhir, M.F., Zakaria, N.Z., Tangang, F., 2014. Intermonsoon variation of physical characteristics and current circulation along the east coast of Peninsular Malaysia. Int. J. Oceanogr. 1—9. https://doi.org/10.1155/2014/527587

Nelson, N.B., Siegel, D.A., Michaels, A.F., 1998. Seasonal dynamics of colored dissolved material in the Sargasso Sea. Deep Sea Res. Pt. I 45 (6), 931—957. https://doi.org/10.1016/S0967-0637(97)00106-4

Nelson, N.B., Siegel, D.A., Carlson, C.A., Swan, C., Smethie, W.M., Khatiwala, S., 2007. Hydrography of chromophoric dissolved organic matter in the North Atlantic. Deep Sea Res. Pt. I 54 (5), 710—731. https://doi.org/10.1016/j.dsr.2007.02.006

Nima, C., Frette, Ø., Hamre, B., Stamnes, J.J., Chen, Y.C., Sørensen, K., Norli, M., Xing, Q., Muyimbwa, Y.C., Sseny-onga, T., Stamnes, K.H., Erga, S.R., 2019. CDOM absorption properties of natural water bodies along extreme environmental gradients. Water 11 (10), 1—19. https://doi.org/10.3390/w11101988

Osburn, C.L., O'Sullivan, D.W., Boyd, T.J., 2009. Increases in the longwave photobleaching of chromophoric dissolved organic matter in coastal waters. Limnol. Oceanogr. 54 (1). https://doi.org/10.4319/lo.2009.54.1.0145

Osburn, C.L., Stedmon, C., 2011. Linking the chemical and optical properties of dissolved organic matter in the Baltic-North Sea transition zone to differentiate three allochthonous inputs. Mar. Chem. 126, 281—294. https://doi.org/10.1016/j.marchem.2011.06.007

Osburn, C.L., Handsel, L.T., Mikan, M.P., Paerl, Montgomery, M.T., 2012. Fluorescence tracking of dissolved and particulate organic matter quality in a river-dominated estuary. Environ. Sci. Technol. 46 (16), 8628—8636. https://doi.org/10.1021/es3007723

Pavlov, A.K., Stedmon, C.A., Semushin, A.V., Martma, T., Ivanov, B.V., Kowalczuk, P., Granskog, M.A., 2016. Linkages between the circulation and distribution of dissolved organic matter in the White Sea. Arctic Ocean. Cont. Shelf Res. 119, 1—13. https://doi.org/10.1016/j.csr.2016.03.004

Sanyal, P., Ray, R., Paul, M, Gupta, V.K., Acharya, A., Bakshi, S., Jana, T.K., Mukhopadhyay, S.K., 2020. Assessing the Dynamics of Dissolved Organic Matter (DOM) in the Coastal Environments Dominated by Mangroves. Indian Sundarbans. Front. Earth Sci. 8, 1—21. https://doi.org/10.3389/feart.2020.00218

Shank, G.C., Evans, A., 2011. Distribution and photoreactivity of chromophoric dissolved organic matter in northern Gulf of Mexico shelf waters. Cont. Shelf Res. 31, 1128—1139. https://doi.org/10.1016/j.csr.2011.04.009

Shanmugam, P., Varunan, T., Jaiganesh, S.N.N., Sahay, A., Chauhan, P., 2016. Optical assessment of colored dissolved organic matter and its related parameters in dynamic coastal water systems. Estuar. Coast. Shelf Sci. 175, 126—145. https://doi.org/10.1016/j.ecss.2016.03.020

Sholkovitz, E.R., 1976. Flocculation of dissolved organic and inorganic matter during the mixing of river water and seawater. Geochim. Cosmochim. Acta 40 (7), 831—845. https://doi.org/10.1016/0016-7037(76)90035-1

Spencer, R.G.M., Hernes, P.J., Ruf, R., Baker, A., Dyda, R.Y., Stubbins, A., Six, J., 2010a. Temporal controls on dissolved organic matter and lignin biogeochemistry in a pristine tropical river, Democratic Republic of Congo. J. Geophys. Res. 115 (G03013), 1—12. https://doi.org/10.1029/2009JG001180

Stedmon, C.A, Markager, S., 2001. The optics of chromophoric dissolved organic matter (CDOM) in the Greenland Sea: An algorithm for differentiation between marine and terrestrially derived organic matter. Limnol. Oceanogr. 46 (8), 2087—2093. https://doi.org/10.4319/lo.2001.46.8.2087

Stedmon, C.A., Markager, S., 2005. Resolving the variability in dissolved organic matter fluorescence in a temperate estuary and its catchment using PARAFAC analysis. Limnol. Oceanogr. 50 (2), 686—697. https://doi.org/10.4319/lo.2005.50.2.0686

Stedmon, C.A., Osburn, C.L., Kragh, T., 2010. Tracing water mass mixing in the Baltic — North Sea transition zone using the optical properties of coloured dissolved organic matter. Estuar. Coast. Shelf Sci. 87 (1), 156—162. https://doi.org/10.1016/j.ecss.2009.12.022

Stedmon, C.A., Amon, R.M.W., Rinehart, A.J., Walker, S.A., 2011. The supply and characteristics of colored dissolved organic matter (CDOM) in the Arctic Ocean: Pan Arctic trends and differences. Mar. Chem. 124 (1—4), 108—118. https://doi.org/10.1016/j.marchem.2010.12.007

Stedmon, C.A., Granskog, M.A., Dodd, P.A., 2015. An approach to estimate the freshwater contribution from glacial melt and precipitation in East Greenland shelf waters using colored dissolved organic matter (CDOM). J. Geophys. Res. 120 (2), 1107—1117. https://doi.org/10.1002/2014JC010501

Teong, K.V., Sukarno, K., Chang, J.H.W., Chee, F.P., Ho, C.M., Dayou, J., 2017. The monsoon effect on rainfall and solar radiation in Kota Kinabalu. Trans. Sci. Technol. 4 (4), 460—465.

Twardowski, M.S., Donaghay, P.L., 2001. Separating in situ and terrigenous sources of absorption by dissolved materials in coastal waters. J. Geophys. Res. 106, 2545—2560. https://doi.org/10.1029/1999JC000039

Winter, A.R., Fish, T.A.E., Playle, R.C., Smith, D.S., Curtis, P.J., 2007. Photodegradation of natural organic matter from diverse freshwater sources. Aquat. Toxicol. 84, 215—222. https://doi.org/10.1016/j.aquatox.2007.04.014

Xie, H., Aubry, C., Bélanger, S., Song, G., 2012. The dynamics of absorption coefficients of CDOM and particles in the St. Lawrence estuarine system: Biogeochemical and physical implications. Mar. Chem. 128—129, 44—56. https://doi.org/10.1016/j.marchem.2011.10.001